Chinese Chemical Letters 36 (2025) 110478

Contents lists available at ScienceDirect

Chinese Chemical Letters

journal homepage: www.elsevier.com/locate/cclet

Hyperforatone A, the 1,8-*seco* rearranged polycyclic polyprenylated acylphloroglucinol with a unique bicyclo[5.4.0]undecane core from *Hypericum perforatum*

Wu-Yang Liu[a], Xin-Xiang Lei[b], Wen-Ji Wang[a], Jun-Mian Tian[a,*], Yu-Qi Gao[a,*], Jin-Ming Gao[a,*]

[a] Shaanxi Key Laboratory of Natural Products & Chemical Biology, College of Chemistry & Pharmacy, Northwest A&F University, Yangling 712100, China
[b] School of Pharmaceutical Sciences, South-Central Minzu University, Wuhan 430074, China

ARTICLE INFO

Article history:
Received 24 July 2024
Revised 14 September 2024
Accepted 19 September 2024
Available online 20 September 2024

Keywords:
Hypericum perforatum
Meroterpenoids
1,8-*Seco* PPAP
Density functional theory calculations
Anti-neuroinflammatory activity

ABSTRACT

Hyperforatone A (**1**), the 1,8-*seco* rearranged polycyclic polyprenylated acylphloroglucinol, possessed an unusual bicyclo[5.4.0]undecane skeleton bearing a 5/7/6/5 ring system, and two known biosynthetically related precursors (**2** and **3**) were isolated from *Hypericum perforatum* (St. John's wort). The structure and absolute configuration were unambiguously confirmed by a combination of comprehensive spectroscopic data, computational methods including residual dipolar couplings (RDCs), and X-ray crystallography. Density functional theory (DFT) calculations revealed that the cationic cyclization reaction was key to proposed formation mechanism for hyperforatone A. Furthermore, *in vitro* and *in vivo* experiments demonstrated that compound **1** was a potential anti-neuroinflammatory agent.

Polycyclic polyprenylated acylphloroglucinols (PPAPs) are a special secondary metabolites from the genus *Hypericum*. Acylphloroglucinol core decorated with prenyl and isoprenyl groups can further be oxidized and cyclized to build the complexity and diversity of PPAPs [1,2]. So far >1000 members of the PPAPs have been reported, of which the majority is the typical [3,3,1]nonane-2,4,9-trione core PPAPs [3]. Biosynthetically, bicyclic PPAPs can be further cyclized to caged PPAPs or be oxidized to open the ring to generate *seco*-PPAPs [2]. The *seco*-PPAPs were considered to be formed by the cleavage of chemical bonds at different positions, including 1,2-*seco*, 2,3-*seco*, 3,4-*seco*, 1,9-*seco*, 1,2;4,5-*diseco* [2,4–6]. Around 40 intriguing architectures of *seco*-PPAPs were characterized [7].

Recently, diverse carbon skeletons of PPAPs were continuously reported from *H. perforatum* (St John's wort), an antidepressive traditional chinese medicine, and other *hypericum* plants, such as hyperfol A, hyperforen A, hymoins A–C and monosescinol A [8–13]. As part of our continuing search for novel bioactive substances from *Hypericum* plants [14–18], chemical investigation on the EtOH extract of the aerial parts of *H. perforatum* led to the discovery of hyperforatone A (**1**), as well as two known precursors, 3-hydroxyhyperforin-3,9-hemiketal (**2**) [19] and hyphenrone A (**3**) [20]. Compound **1** was a 1,8-*seco* rearranged PPAP bearing a rare bicyclo[5.4.0]undecane carbon skeleton (Fig. 1). In preparing process for this paper, we found that hyperforatone A (**1**) was the same structure as hyperlanin A [21], a PPAP originally isolated from a distinct plant, *Hypericum lancasteri*. Noteworthily, we performed an accurate identification of the relative and absolute configurations using residual dipolar couplings (RDCs), nuclear magnetic resonance spectroscopy (NMR) and electronic circular dichroism (ECD) calculations due to the presence of multiple quaternary stereocenters in compound **1**. Moreover, density functional theory (DFT) calculations were used to reveal a reasonable formation mechanism for carbocation process of **1** compared to the radical reaction. In addition, neuroinflammation is one of the crucial factors in the development of depression. Compound **1** displayed a significant anti-neuroinflammatory effect in lipopolysaccharide (LPS)-induced BV-2 microglial cells and zebrafish model, thereby providing new additional evidence for the antidepressant effect of *H. perforatum*. Herein, we describe the structural elucidation, hypothetical biogenetic pathway, and biological activity of the isolation (**1**).

Hyperforatone A (**1**) was isolated as colorless crystals. Its molecular formula was assigned as $C_{35}H_{52}O_5$ according to pseudomolecular ion peak at *m/z* 553.3884 $[M+H]^+$ (calcd. for $C_{35}H_{53}O_5$,

* Corresponding authors.
E-mail addresses: tianjunmian@nwsuaf.edu.cn (J.-M. Tian), gyq1225@nwu.edu.cn (Y.-Q. Gao), jinminggao@nwsuaf.edu.cn (J.-M. Gao).

https://doi.org/10.1016/j.cclet.2024.110478
1001-8417/

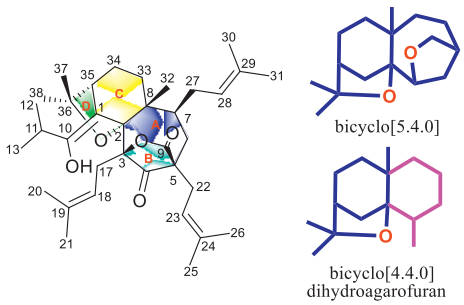

Fig. 1. Chemical structure of **1**.

553.3887) in positive high resolution electrospray ionization mass spectroscopy (HR-ESI-MS) spectrum, corresponding to 10 degrees of unsaturation. Three olefinic protons [δ_H 4.96 (1H, overlap), 4.93 (1H, overlap) and 4.77 (1H, t, J = 7.8 Hz)], two characteristic doublet methyls of isopropyl [δ_H 1.16 (d, J = 6.6 Hz), 1.13 (d, J = 6.6 Hz)], and nine singlet methyls (δ_H 1.68–1.04) were presented in the ^{1}H NMR spectrum. In the ^{13}C NMR and distortionless enhancement by polarization transfer (DEPT) 135 spectra, 35 carbon signals were assigned, including 11 methyls, 6 methylenes, 6 methines, and 12 quaternary carbons. Among them, a ketone (δ_C 205.8), an ester carbonyl (δ_C 174.3), three isoprenyl groups (δ_C 138.0, 136.2, 133.3, 123.3, 117.8, 115.9, 31.2, 31.2, 29.3, 26.4, 26.2, 26.0, 18.1, 18.1, 18.0), two olefinic carbons (δ_C 148.5, 110.0), three oxygenated carbons (δ_C 93.2, 90.0, 81.3), and an isopropyl group (δ_C 31.8, 20.5, 20.4) were distinguished (Table 1). Since **1** had 10 degrees of unsaturation, while a ketone, an ester carbonyl, and four olefinic bonds simply accounted for 6 degrees of unsaturation, **1** should bear another four rings. The above analysis showed that **1** was a tetracyclic PPAP-derivative.

The completed assignment for protons and carbons of **1** was addressed by 2D NMR experiments (Fig. 2). From ^{1}H–^{1}H correlation spectroscopy (COSY) experiment, five fragments, **a** (H_2–27/H-28), **b** (H_2–22/H-23), **c** (H_2–17/H-18), **d** (H_3–12/H-11/H_3–13) and **e** (H_2–33/H_2–34/H-35), were observed. The heteronuclear multiple bond correlation (HMBC) correlations from H_2–17 to C-3/C-4, from H_2–22 to C-4/C-5/C-6, from H_2–27 to C-6/C-7, and from H_2–6 to C-4/C-5/C-7/C-8 undoubtedly confirmed that the connectivity of C-3/C-4/C-5/C-6/C-7/C-8. The 2–hydroxyl-3-methyl-1,1-disubstuted-1-butenyl group at C-1 position was confirmed by the HMBC correlations from the proton of 10–OH to C-1/C-10/C-11 and

Table 1
^{1}H (500 MHz) and ^{13}C NMR (125 MHz) data of **1** in $CDCl_3$.

No.	δ_H (J in Hz)	δ_C	No.	δ_H (J in Hz)	δ_C
1		110.0	22a	2.47 dd (14.6, 7.5)	31.2
2		90.0	22b	2.40 dd (14.6, 7.5)	
3		93.2	23	4.93 overlap	117.8
4		205.8	24		136.2
5		53.2	25	1.66 s	18.0
6	a 1.81, b 1.61 m	37.5	26	1.65 s	26.2
7	1.72 m	41.8	27	a 2.15, b 1.62 m	29.3
8		49.3	28	4.96 overlap	123.3
9		174.3	29		133.3
10		148.5	30	1.53 s	18.1
11	2.72 m	31.8	31	1.68 s	26.0
12	1.16 d (6.6)	20.5	32	1.04 s	16.3
13	1.13 d (6.6)	20.4	33	a 1.81, b 1.26 m	37.5
17a	3.00 dd (14.7, 6.8)	31.2	34	a 1.82, b 1.65 m	27.7
17b	2.64 dd (14.7, 8.5)		35	2.53 overlap	49.6
18	4.77 t (7.8)	115.9	36		81.3
19		138.0	37	1.22 s	30.4
20	1.63 s	18.1	38	1.32 s	22.2
21	1.63 s	26.4	OH	6.98	

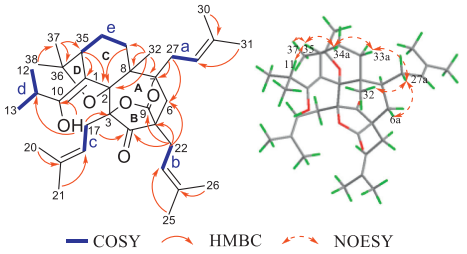

Fig. 2. Key 2D NMR correlations for **1**.

H-11 to C-1/C-10. The two methyls (δ_C 30.4, 22.2; δ_H 1.22, 1.32) were located at oxygenated C-36 by the HMBC correlations of H_3–38 to C-36/C-37 and H_3–37 to C-35. The HMBC correlations from H_3–32 to C-33, from H_2–33 to C-2, and from H-35 to C-1/C-2/C-10/C-33/C-34 conclusively indicated that the connections of C-1/C-2/C-8/C-33/C-34/C-35. The fused two rings **A** and **C** through the bridge of C-2/C-8 bond were confirmed by critical the HMBC correlations from H_b-17 to C-2 and H_3–32 to C-2/C-7/C-8. An internal ester bridge between C-3 and C-5 (ring **B**) was deduced by the HMBC correlation from H_2–22 to C-9, along with the characteristic downfield chemical shifts of C-3 at δ_C 93.2 and C-5 at δ_C 53.2. In addition, ring **D** was formed *via* an ether bond which connected C-2 at δ_C 90.0 with C-36 at δ_C 81.3.

The relative configuration of **1** was determined by the analysis of its nuclear overhauser effect spectroscopy (NOESY) spectrum (Fig. 2). The correlations of H_3–32/H_a-27/H_a-33, H_a-33/H_a-34/H-35, H_a-27/H_a-6 and H-35/H_3–37 suggested that H_a-27, H_3–32, H_a-33, H_a-34, H-35 and H_3–37 were in the same orientation. In addition, the Z configuration of $\Delta^{1(10)}$ double bond was determined by the NOE correlation of H-35/H-11. RDCs were a powerful tool for the relative configuration analysis of complicated natural products [22]. To further validate the above assignment for **1**, RDCs were successfully applied to determine its relative configuration. Total couplings ($^1T_{CH}$), scalar couplings ($^1J_{CH}$), and residual dipolar couplings ($^1D_{CH}$) were calculated in a 2.9% oligopeptide amphiphile (OPA) aligned medium, and the corresponding Q factors were used to evaluate the possibility of relative configurations. The eight possible diastereomeric configurations were obtained. The (2*R**,3*R**,5*S**,7*R**,8*S**,35*S**)–**1**a had the best fitting with the lowest Q factor of 0.012 (Fig. 3). Moreover, the calculated ^{13}C NMR chemical shifts of (2*R**,3*R**,5*S**,7*R**,8*S**,35*S**)-truncation of **1** was quite consistent with the experimental chemical shifts, with a good linear correlation coefficient (R^2, 0.9983), a lower mean absolute error (MAE, 1.7) and a lower corrected mean absolute error (CMAE, 1.7) (Tables S4 and S5 in Supporting information).

The absolute configuration was further confirmed by the ECD calculation. The calculated ECD spectrum of (2*S*,3*S*,5*R*,7*S*,8*R*,35*R*)–**1** was fully matched with the experimental ECD spectrum with positive Cotton effect around 200 and 225 nm and negative Cotton

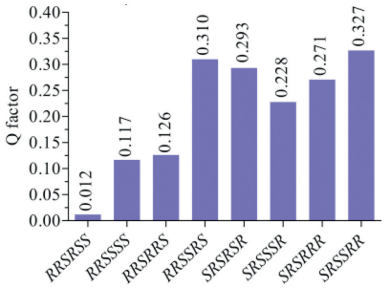

Fig. 3. Corresponding Q factors of the RDCs for the eight possible diastereomeric configurations of **1**.

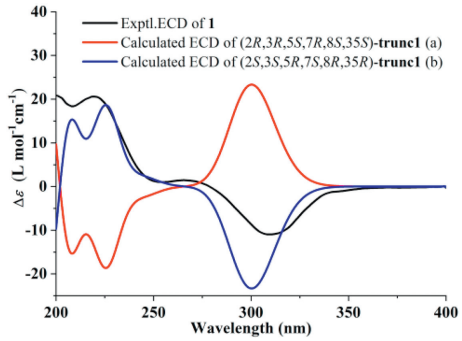

Fig. 4. Calculated and experimental ECD spectra of **1**.

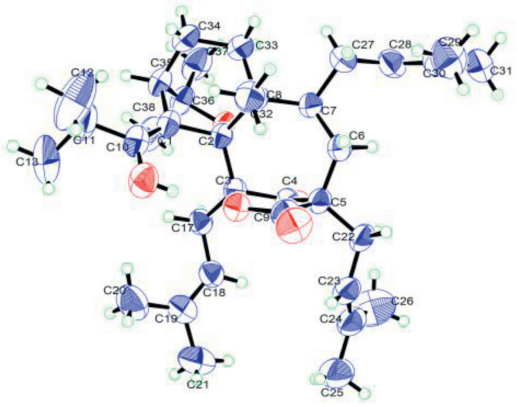

Fig. 5. Oak ridge thermal ellipsoid plot (ORTEP) drawing of **1**.

effect around 310 nm (Fig. 4). Finally, the orthorhombic crystals of **1** were obtained from acetone, and the single-crystal X-ray diffraction analysis (Cu Kα) [Flack parameter = −0.06(6)] unequivocally confirmed the structural assignments (Fig. 5). Thus, the absolute configuration of **1** was clarified as 2*S*,3*S*,5*R*,7*S*,8*R*,35*R*.

To the best of our knowledge, two biosynthetic pathways, cationic and radical cyclization, are involved in the carbon skeleton rearrangement of PPAPs [7,23–25]. To assess the feasibility of 5/7/6/5 ring system formation in the biosynthesis of **1**, the chemical computation was performed.

Based on the calculated results of the cationic process (Scheme 1 and Fig. 6), **1** might derive from hyperforin (HF), the

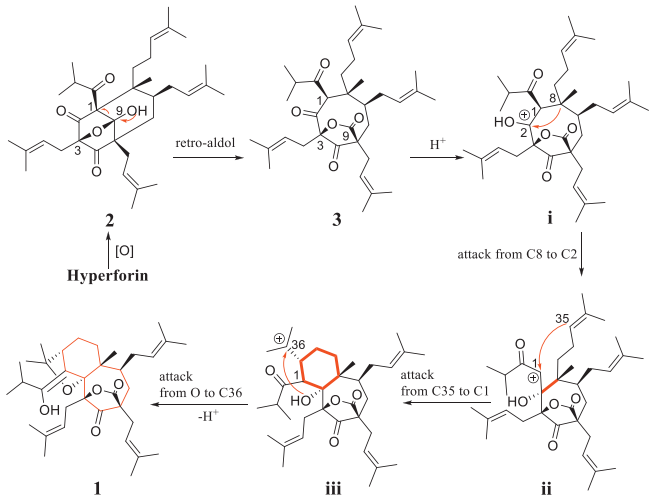

Scheme 1. Plausible biosynthetic pathway of **1**.

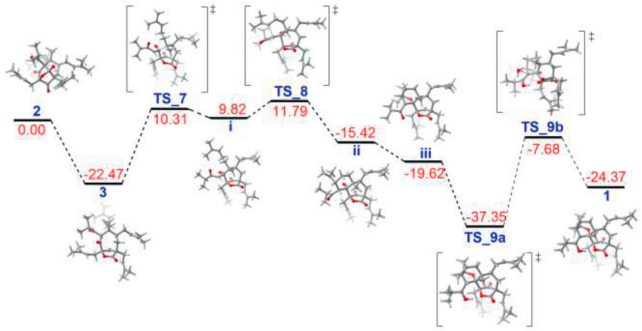

Fig. 6. The calculated energy profile (kcal/mol) with DFT for the carbocation process of compound **1**.

antidepressant constituent of St John's wort, *via* a crucial intermediate hemiketal **2**. Then, **2** cleaved the C-1/C-9 bond *via* a retro-aldol mechanism to form a five-membered lactone fragment (B ring) of **3** with free energy of −22.47 kcal/mol. The carbonyl carbon (C-2) occurred to protonation. Then the key intermediate (**i**) of the seven-membered A ring was produced by the heterolytic cleavage of the C-1/C-8 bond and the formation of the C-2/C-8 bond which the *tert*–alkyl anion of C-8 attacked to the carbonyl cation of C-2 [26,27]. The process needed to overcome the activation barrier (ΔG = 32.78 kcal/mol). It was easier to form the C ring through the pair of electrons of the olefinic bond at C-35 attacking to the cation of C-1 to afford the intermediate **ii** by transition structure (TS_8) with an activation free energy barrier of 1.97 kcal/mol. It tended to form the D ring from intermediate **ii** to intermediate **iii**, because of the distance (3.65 Å) between the oxygen at C-2 and the carbon of C-36, a barrier-free and exergonic step (ΔG = −4.20 kcal/mol). Finally, **1** was obtained by the ketone/alcohol conversion, which the process included protonation of the carbonyl O under acidic condition (TS_9a with a free energy of −37.35 kcal/mol) and deprivation of the proton at C-1 position (TS_9b with a free energy of −7.68 kcal/mol).

A radical process of **1** was also speculated and calculated with the DFT (Scheme S1 and Fig. S17 in Supporting information). The radical transition state (TS_13) might be produced under irradiation conditions, which triggered the radical reaction chain. As we all know, the radical intermediate might undergo β-fragmentation (1,8-*seco*) to produce a *tert*–alkyl radical and an enol anion substituent [28]. Then, the *tert*–alkyl radical (C-8) might add to the α-carbon radical (C-2) of the enol anion group to produce the seven-membered A ring (intermediate **iv**) [29,30]. However, the steps from **3** to intermediate **iv** proceed through overcoming activation free energy of 78.34 kcal/mol. The formation of the C ring (intermediate **v**) could be produced by two steps of the radical cyclization *via* transition structure (TS_14) with barrier of 20.35 kcal/mol. The formation of D ring (intermediate **vi**) was a highly exergonic step (ΔG = −72.60 kcal/mol). For the ketone/alcohol conversion, the protonation of TS_9a was barrier-free and exergonic, and the proton at C-1 position was deprived through an activation barrier (ΔG = 45.03 kcal/mol). At this level of calculation, it was concluded that the biosynthetic proposal for the formation of **1** through the cationic cyclization reaction was feasible compared to the radical reaction.

We evaluated the anti-neuroinflammatory activities of compounds **1**–**3** and HF using LPS-induced BV-2 microglial cells model and *S*-methylisothiourea (SMT) as a positive control. The results showed that compound **1** and HF exhibited moderate inhibition of nitric oxide (NO) production with half maximal inhibitory concentration (IC_{50}) values of 31.00 and 21.68 μmol/L, respectively. The IC_{50} value of SMT was 5.93 μmol/L. Compounds **2** and **3** showed no significant NO inhibition with IC_{50} values greater than 50 μmol/L

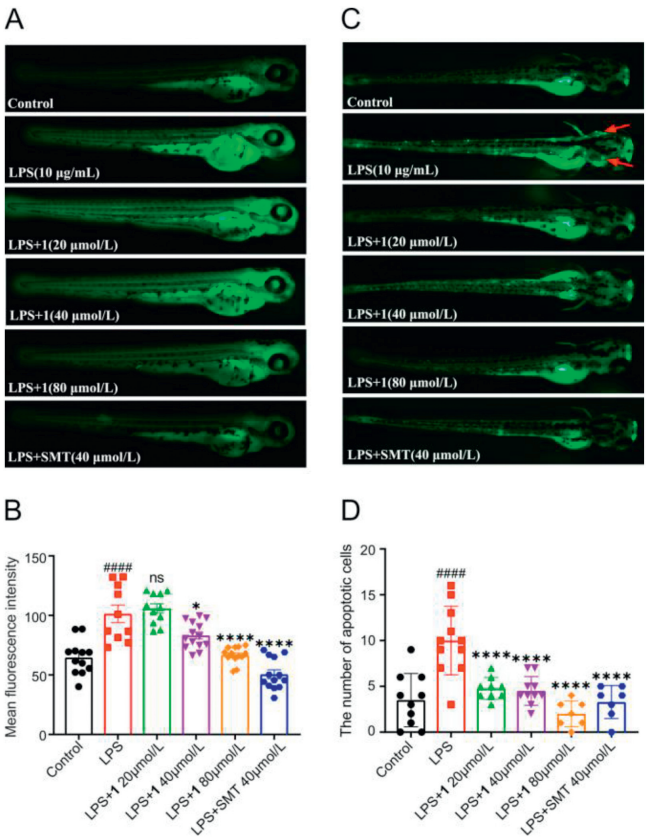

Fig. 7. Effects of compound **1** on NO production and neuronal apoptosis in LPS-induced zebrafish. (A, C) NO production and neuronal apoptosis were imaged using fluorescence microscopy. (B, D) Mean fluorescence intensity and the number of apoptotic cells were quantified using Image J. $^{\#\#\#\#}P < 0.0001$ *vs.* control (DMSO) group; $^{*}P < 0.05$, $^{****}P < 0.0001$ *vs.* LPS group (ns, no significance).

(Table S12 in Supporting information). None of these tested drugs showed significant cytotoxicity against BV-2 cells at the tested concentrations (Fig. S20 in Supporting information). In addition, we tested the effect of each drug at 40 μmol/L on LPS-induced NO production and the number of apoptotic nerves in the head using zebrafish larvae. The results showed that compound **1**, HF and SMT significantly inhibited LPS-induced NO production and markedly reduced the number of neuronal apoptosis in the head of zebrafish larvae. Compounds **2** and **3** did not show significant inhibitory activity at this concentration (Figs. S22 and S23 in Supporting information). This is basically consistent with the results of intracellular activity.

Inducible nitric oxide synthase (iNOS) and cyclooxygenase-2 (COX-2) play key roles in the production of pro-inflammatory mediators. Western blot analysis revealed that **1** downregulated the expression of iNOS and COX-2 in LPS-stimulated BV-2 microglial cells (Figs. S24B–D in Supporting information). In addition, we measured NO production and neuronal apoptosis in LPS-induced zebrafish. As shown in Figs. 7A and B, NO production was significantly increased when zebrafish larvae were stimulated with LPS. Conversely, NO level was notably reduced in a dose-dependent manner after treatment with compound **1**. Furthermore, **1** significantly reduced the neuronal apoptosis in the head of zebrafish after LPS stimulation (Figs. 7C and D). The results in zebrafish demonstrated that **1** exerted anti-neuroinflammatory effects by inhibiting NO production and neuronal apoptosis.

In summary, a novel PPAP, hyperforatone A (**1**) was isolated from the aerial parts of *H. perforatum*. Compound **1** was a bicyclo[5.4.0]undecane architecture by 1,8-*seco* rearranged reactions. The cationic cyclization was favored to construct rare carbon skeleton by DFT calculations. Its structure may attract particular attention of organic synthesis and phytochemists. In addition, **1** showed a moderate anti-neuroinflammatory effect in LPS-induced BV-2 microglial cells and zebrafish.

Declaration of competing interest

The authors declare that they have no known competing financial interests or personal relationships that could have appeared to influence the work reported in this paper.

CRediT authorship contribution statement

Wu-Yang Liu: Writing – original draft, Visualization, Software, Methodology, Formal analysis, Data curation, Conceptualization. **Xin-Xiang Lei:** Software, Methodology, Data curation. **Wen-Ji Wang:** Software, Methodology, Investigation, Data curation. **Jun-Mian Tian:** Writing – review & editing, Supervision, Methodology, Data curation. **Yu-Qi Gao:** Writing – review & editing, Validation, Supervision. **Jin-Ming Gao:** Writing – review & editing, Supervision, Project administration, Funding acquisition.

Acknowledgments

This work was financially supported by the National Natural Science Foundation of China (Nos. 22077102, 32201249) and the Science and Technology Program of Gansu Province (No. 22YF7GA046). We also greatly acknowledge high performance computing (HPC) of Northwest A&F University for the density functional theory calculations carried out in this work.

Supplementary materials

Supplementary material associated with this article can be found, in the online version, at doi:10.1016/j.cclet.2024.110478.

References

[1] R. Ciochina, R.B. Grossman, Chem. Rev. 106 (2006) 3963–3986.
[2] X.W. Yang, R.B. Grossman, G. Xu, Chem. Rev. 118 (2018) 3508–3558.
[3] Z.H. Xu, R.B. Grossman, Y.F. Qiu, et al., J. Nat. Prod. 85 (2022) 2845–2855.
[4] W.J. Lu, Y.Q. Zhang, Y.W. Li, et al., Chin. Chem. Lett. 33 (2022) 4121–4125.
[5] R.D. Liu, Y.L. Su, J.B. Yang, et al., Phytochemistry 142 (2017) 38–50.
[6] S.S. Xie, C.X. Qi, Y.L. Duan, et al., Org. Chem. Front. 7 (2020) 1349–1357.
[7] Y.L. Hu, K. Hu, L.M. Kong, et al., Org. Lett. 21 (2019) 1007–1010.
[8] Y. Guo, N. Zhang, C. Chen, et al., J. Nat. Prod. 80 (2017) 1493–1504.
[9] H. Bridi, G.de.C. Meirelles, G.L. von Poser, Phytochemistry 155 (2018) 203–232.
[10] H.Y. Lou, F.W. Ma, P. Yi, et al., J. Arab. J. Chem. 15 (2022) 104057.
[11] H.Y. Lou, Y.N. Li, P. Yi, et al., Org. Lett. 22 (2020) 6903–6906.
[12] C.M. Yuan, Y.R. Zeng, L. Huang, et al., Chin. Chem. Lett. 36 (2024) 109859.
[13] Z.Y. Shi, J. Yin, Y. Xiao, et al., Chin. Chem. Lett. 35 (2024) 109458.
[14] X.T. Yan, Z. An, D. Tang, et al., RSC Adv. 8 (2018) 26646–26655.
[15] X.T. Yan, Z. An, Y. Huangfu, et al., Phytochemistry 159 (2019) 65–74.
[16] J.Y. Xie, P.F. Li, X.T. Yan, et al., Commun. Chem. 7 (2024) 1.
[17] X.T. Yan, J.X. Chen, Z.X. Wang, et al., J. Nat. Prod. 86 (2023) 119–130.
[18] J.Y. Xie, Z.X. Wang, W.Y. Liu, et al., J. Nat. Prod. 86 (2023) 1910–1918.
[19] L. Verotta, G. Appendino, J. Jakupovic, et al., J. Nat. Prod. 63 (2000) 412–415.
[20] X.W. Yang, Y. Ding, J.J. Zhang, et al., Org. Lett. 16 (2014) 2434–2437.
[21] J.Q. You, Y.Q. Jin, M.Y. Li, et al., Chin. J. Chem. 42 (2024) 2180–2186.
[22] W.B. Han, Y.J. Zhai, R. Zhang, et al., Angew. Chem. Int. Ed. 62 (2023) e202300773.
[23] W.J. Xu, P.F. Tang, W.J. Lu, et al., Org. Lett. 21 (2019) 8558–8562.
[24] N.N. Jiang, Y.S. Ye, X. Liu, et al., Org. Lett. 25 (2024) 8965–8969.
[25] X.Y. Jia, Y.M. Wu, C. Lei, et al., Chin. Chem. Lett. 31 (2020) 1263–1266.
[26] J.F. Zong, Z. Hu, Y.Y. Shao, et al., Org. Lett. 22 (2022) 2797–2800.
[27] Y.L. Duan, Y. Guo, Y.F. Deng, et al., J. Org. Chem. 87 (2022) 6824–6831.
[28] C. Janine, Photoinduced electron tranfer in radical reactions, Vol. 1, in: R. Philippe, P.S. Mukund (Eds.), Radicals in Organic Synthesis, Wiley-Vch Press: Strauss Offsetdruck Gmbh Press, Mörlenbach, 2001, pp. 245.
[29] L. Canonica, B. Danieli, G. Lesma, et al., Helv. Chim. Acta 70 (1987) 701–716.
[30] K. Cen, J.J. Bao, X.D. Wang, et al., J. Am. Chem. Soc. 146 (2024) 6481–6486.